ACS Energy LETTERS

http://pubs.acs.org/journal/aelccp

PERSPECTIVE

Deformation during Electrosorption and Insertion-Type Charge Storage: Origins, Characterization, and Design of Materials for High Power

Veronica Augustyn,* Ruocun Wang, Nina Balke, Matt Pharr, and Craig B. Arnold

Cite This: *ACS Energy Lett.* 2020, 5, 3548−3559

Read Online

ACCESS | Metrics & More | Article Recommendations

ABSTRACT: **Ion electrosorption and insertion form the basis of two commercialized electrochemical energy storage technologies: electric double-layer capacitors and lithium ion batteries. These processes are also of interest for emerging applications in water treatment, critical element extraction, and neuromorphic computing. The kinetics of electrosorption and insertion are intimately related to the mechanical deformation of the host material. This Perspective discusses the following: (1) similarities and differences in the deformation response of materials due to ion electrosorption and insertion, (2) correlation between mechanical and electrochemical response via several *operando* techniques, and (3) how the understanding of deformation can guide the design of new electrosorption and ion insertion materials with faster kinetics.**

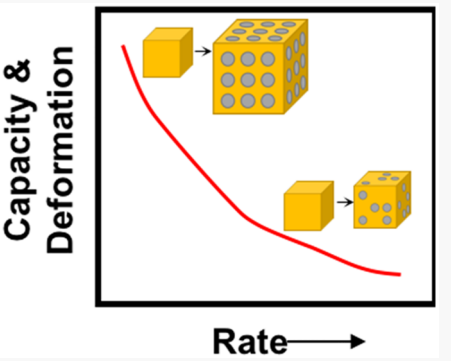

Electrochemically driven adsorption (electrosorption) and insertion of ions into solid-state materials form the basis of two commercialized electrochemical energy storage (EES) technologies: electric double-layer capacitors (EDLCs)[1] and lithium-ion batteries (LIBs).[2−4] Figure 1 illustrates the device schematic for both of these: in an EDLC, energy storage occurs via ion electrosorption onto high surface area carbon electrodes[5] while in a LIB, energy storage occurs via Li-ion insertion into anode and cathode hosts.[6] Electrosorption and insertion of ions are also considered for emerging applications, such as desalination,[7] ion separation,[8] recovery of elements,[9] and neuromorphic computing.[10,11] In all of these applications, the power is fundamentally limited by the kinetics associated with ion electrosorption and insertion into a solid-state host electrode. It is highly desirable, if not necessary, for such devices to operate on minute or even second time scales, which drives the search for electrosorption and insertion hosts with fast kinetics.

At first glance, there appear to be few similarities between ion electrosorption, an electrostatic/nonfaradaic process, and ion insertion, a chemical/faradaic process that involves ion desolvation, electron transfer, and solid-state diffusion. However, the degree of interaction between an ion and electrode host lies on a continuum, with nonfaradaic electrosorption and desolvated ion insertion at either end. This is why, for example, insertion reactions in LIBs can be described by modified adsorption isotherms.[12,13] Moreover, these processes share a common feature that upon charge storage, the host solid-state electrode undergoes structural rearrangements that lead to deformation.[14,15] For example, the relative height of an EDLC activated carbon electrode changes up to 1.8% because of the electrosorption of ions from the electrolyte (Figure 1C).[16−18] In the case of LIBs, electrochemical cycling can lead to reversible expansion and contraction (Figure 1D).[19] Such dimensional changes primarily arise from the relationship between ion electrosorption or insertion capacity and deformation in the host electrode material. This leads to fundamental coupling between current associated with ion electrosorption and insertion and the dynamic mechanical response of the host electrode that makes it possible to understand kinetics of charge storage from the deformation response. Moreover, the

Received: August 21, 2020
Accepted: October 14, 2020

https://dx.doi.org/10.1021/acsenergylett.0c01823
ACS Energy Lett. 2020, 5, 3548−3559

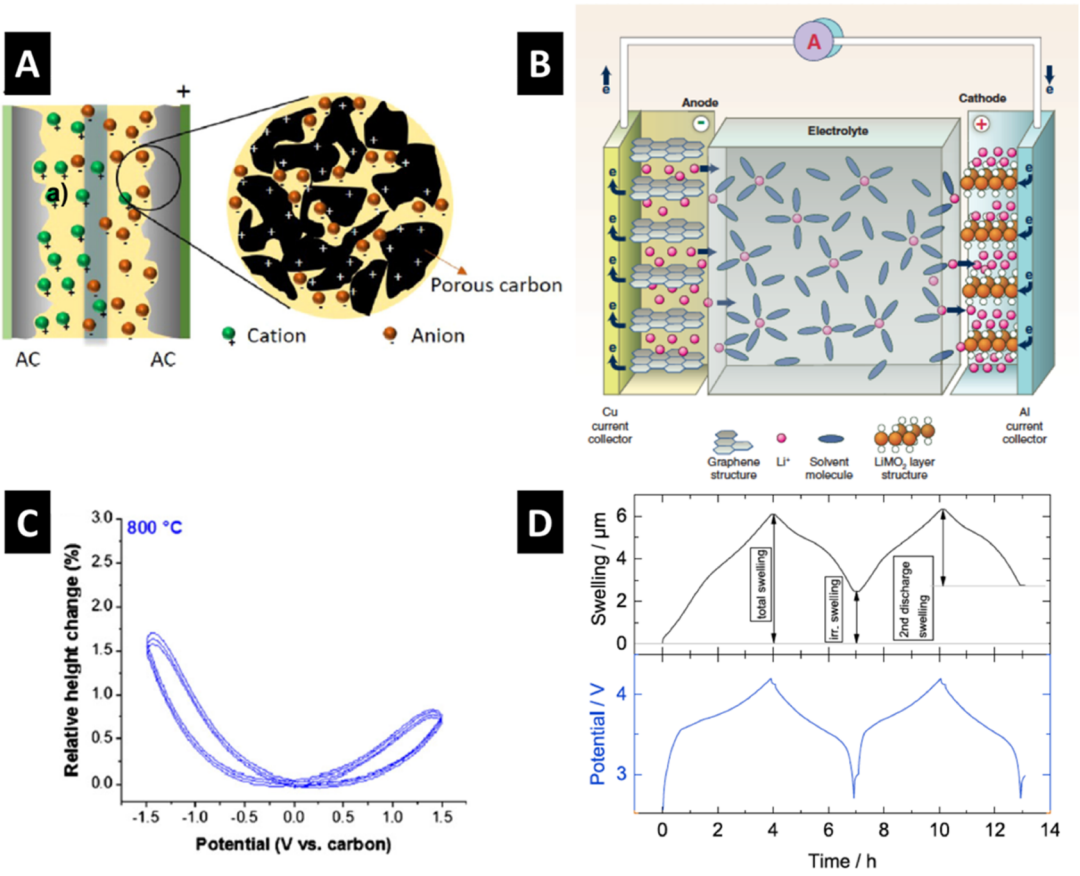

Figure 1. Overview of electrosorption and insertion-type mechanisms and their respective relationships between electrode deformation and charge storage. (A) Schematic of an EDLC, where the inset illustrates ion electrosorption into nano- and subnanometer pores of a high surface area carbon electrode. Adapted from ref 5 with permission from Elsevier. (B) Schematic of a LIB with two insertion-type electrodes as the anode (graphite) and cathode ($LiMO_2$, where M is typically a third-row transition metal such as Co, Ni, or Mn). Adapted from ref 6. Reprinted with permission from AAAS. (C) Electrosorption-induced deformation (as relative height change) of an EDLC electrode in an ionic liquid electrolyte. The asymmetry of the parabolic curve is due to differences in the ionic radii of the cation and anion. Adapted from ref 16 with permission from Elsevier. (D) Swelling (expansion) of a $LiNi_{1/3}Mn_{1/3}Co_{1/3}O_2$/graphite LIB during electrochemical cycling at a rate of C/3 (charge/discharge within 3 h). Adapted from ref 19 with permission from Elsevier.

concept of minimizing the deformation of the electrode while maintaining capacity could lead to new designs for host materials with fast kinetics and long lifetimes.

The purposes of this Perspective are to discuss (1) similarities and differences in the deformation response of materials due to ion electrosorption and insertion, (2) correlations between mechanical and electrochemical responses via several *operando* techniques, and (3) how the understanding of deformation can guide the design of new electrosorption and ion insertion materials with faster kinetics.

> There is fundamental coupling between current associated with ion electrosorption and insertion and the dynamic mechanical response of the host electrode that makes it possible to understand kinetics of charge storage from the deformation response.

Origins of Deformation in Electrosorption and Insertion-Type Charge Storage and Operando Characterization. The close coupling of electrochemical kinetics with mechanical response begins at the atomic scale for both electrosorption and ion insertion and manifests itself across length scales, from local to the cell-level. While smaller than the volume changes that occur during ion insertion, deformation associated with electrosorption is still significant and can be between 1 and 2% depending on the electrode material, electrolyte solvent, and ion.[20] Moreover, if the operating voltage of EDLCs is extended >4 V in order to increase the energy density, the deformation associated with electrosorption will play an even more significant role in the device power and lifetime. Electrosorption into high surface area materials such as activated carbons (>1000 m^2 g^{-1}) involves pores with diameters that approach the desolvated ion size.[21−23] Electrochemical double layer (EDL) formation in such a confined environment, where the pore size essentially matches the desolvated ion size, is significantly different from the EDL formed at a planar interface described by Guoy−Chapman−Stern theory.[22] The lack of space available for the formation of the diffuse layer leads to overlapping EDLs as described by modified Donnan models.[24] Deformation from ion electrosorption can arise from two processes: (1) change in osmotic pressure due to changes in ion concentration at the EDL and (2) variation in bond length due to changes in the electrode density of states arising from electron or hole doping.[25−27]

https://dx.doi.org/10.1021/acsenergylett.0c01823
ACS Energy Lett. 2020, 5, 3548−3559

Molecular dynamic simulations of the pressure effect indicate that deformation arises from forces generated as a result of the van der Waals and Coulombic interactions between the electrosorbed electrolyte ions and the carbon electrode pore walls.[26] These forces generate a pressure on the carbon electrode that depends on the pore size and applied voltage.[18] When the ion size approaches the pore size, the forces on the pore wall depend on the pore size and show an oscillatory behavior.[28] This can lead to observed asymmetries in the electrode volume change when the cations and anions are of different sizes.[16,26]

The insertion of a desolvated ion accompanied by electron transfer, as in LIBs, leads to changes in bond lengths and angles of the host structure, with or without a structural transformation.[14,29,30] The fundamental connection between a faradaic process and mechanical response is evident even with a simple molecule undergoing oxidation, such as ferrocene, which exhibits no change in structure when oxidized to ferricenium but does show lengthening of the Fe−C bond by ∼5%.[31,32] In ion insertion electrodes of extended solid structures, these concerted atomic-scale strains lead to volume changes, stress generation, and even phase transformations.[33−35] If the solid-state diffusion of the inserting species in the host is sluggish, the presence of a concentration gradient in the material can result in diffusion-induced stress between the inserted versus noninserted regions due to spatial mismatches in strain.[36−40] Stresses that develop during insertion or externally applied stresses can affect the total electrochemical potential of the system, which can couple back to alter the insertion kinetics.[41,42] Such effects can be exacerbated because of nonuniformities or other gradients in the system.[43,44] In most systems, compressive stresses develop during insertion, and this tends to slow subsequent insertion kinetics. Rate limitations can also arise from electrochemically induced structural transformations that lead to the nucleation of new structural phases.[45]

From a mathematical standpoint, ion electrosorption and insertion both lead to structural changes, or strains, in the materials where the strain (ε) takes the form

$$\varepsilon = \frac{\delta}{L_0} \tag{1}$$

and δ is the deformation (e.g., change in bond length, $L - L_0$) and L_0 is the original length. In the case of insertion, a proportionality has been observed in several systems between the accumulated charge (Q) and elastic strain as a function of time:[46,47]

$$Q \propto \varepsilon \tag{2}$$

In the case of EDLCs, the strain scales with the square of the charge because of the nature of the ion electrosorption process around the point of zero charge (PZC) and thus[26]

$$Q^2 \propto \varepsilon \tag{3}$$

In simple terms, the deformation scales with the amount of charge storage. In the same manner, the rate of electrode elastic deformation is related to insertion current for cyclic voltammetry experiments with constant sweep rate (dV/dt):[46−48]

$$\frac{dQ}{dt} = I \propto \frac{d\varepsilon}{dt} \tag{4}$$

where t is time and I is current. For galvanostatic charge−discharge tests, the following relationship was observed by Schiffer et al.:[48]

$$\frac{dV}{dQ} \propto \frac{d^2\varepsilon}{dQ^2} \tag{5}$$

Together, these relationships allow for the correlation of mechanical response with *operando* measurement of deformation during ion electrosorption and insertion-type materials.[35,49]

The understanding of electrosorption and insertion mechanics will shed light on whether it is possible to decouple kinetics, which favor open structures with little distortion, from capacity, which favors dense structures with minimal inactive atoms.

Because electrode deformation at the local and cell level is a direct measure of the extent of charge storage, many techniques are available for *operando* characterization of electrode deformation during ion electrosorption and insertion.[50,51] They differ significantly in terms of spatial and temporal resolution as well as ease of implementation. Here we highlight examples from four techniques that are relatively straightforward to implement for *operando* electrochemical characterization: (1) electrochemical dilatometry, (2) digital image correlation (DIC), (3) atomic force microscopy (AFM), and (4) beam curvature techniques. The first three techniques calculate strain via measured electrode deformation and the last technique measures the curvature change of a substrate to obtain the insertion-induced stress in thin-film electrodes. Electrochemical dilatometry measures deformation by measuring strain perpendicular to two parallel pistons or via a linear variable differential transformer (LVDT).[48] DIC compares 2D images of electrodes recorded optically and uses feature displacement to determine strain.[46,52,53] AFM provides a local measurement of nanoscale electrode deformation due to the nanoscale dimensions of an AFM tip, with a spatial resolution of tens of nanometers.[26,47,54,55] Beam curvature techniques, such as the multibeam optical stress sensor (MOSS) approach, measure the curvature of a thin-film electrode on a substrate and convert it to a stress measurement. Standard setups can resolve changes in the radius of curvature down to ∼10 km, which produces typical stress resolutions at the single MPa level. All of these techniques enable high temporal resolution and correlation between the measured strain or stress and electrochemical potential and current. Another important benefit is that the mechanical response could be used as a proxy for electrochemical response in situations where the electrochemical insertion current may be difficult or inaccurate to measure. This can be the case if there are multiple electrochemical processes occurring at the same time (e.g., electrolyte decomposition and ion insertion) or when the sample volume is small, as in single-particle electrochemistry. It should be noted that there are other experimental techniques for strain measurement, including electron microscopy,[56−58] X-ray microscopy,[59−61] X-ray diffraction,[62,63] and electrochemical quartz crystal microbalance.[64,65]

https://dx.doi.org/10.1021/acsenergylett.0c01823
ACS Energy Lett. 2020, 5, 3548−3559

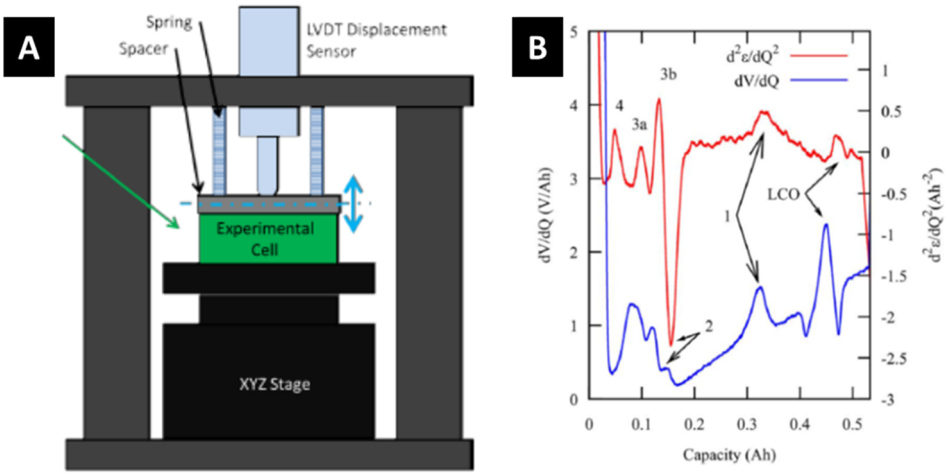

Figure 2. Electrochemical dilatometry of Li-ion pouch cell batteries. (A) Standard LVDT arrangement for strain measurements. (B) Simultaneous measurement of the second derivative of strain with respect to charge and first derivative of voltage with respect to charge showing peak correlation. "LCO" denotes structural transitions associated with Li^+ deintercalation from the cathode ($LiCoO_2$), while the labels 1, 2, 3, and 4 correspond to Li^+ staging transitions in the graphite anode. Adapted from ref 48.

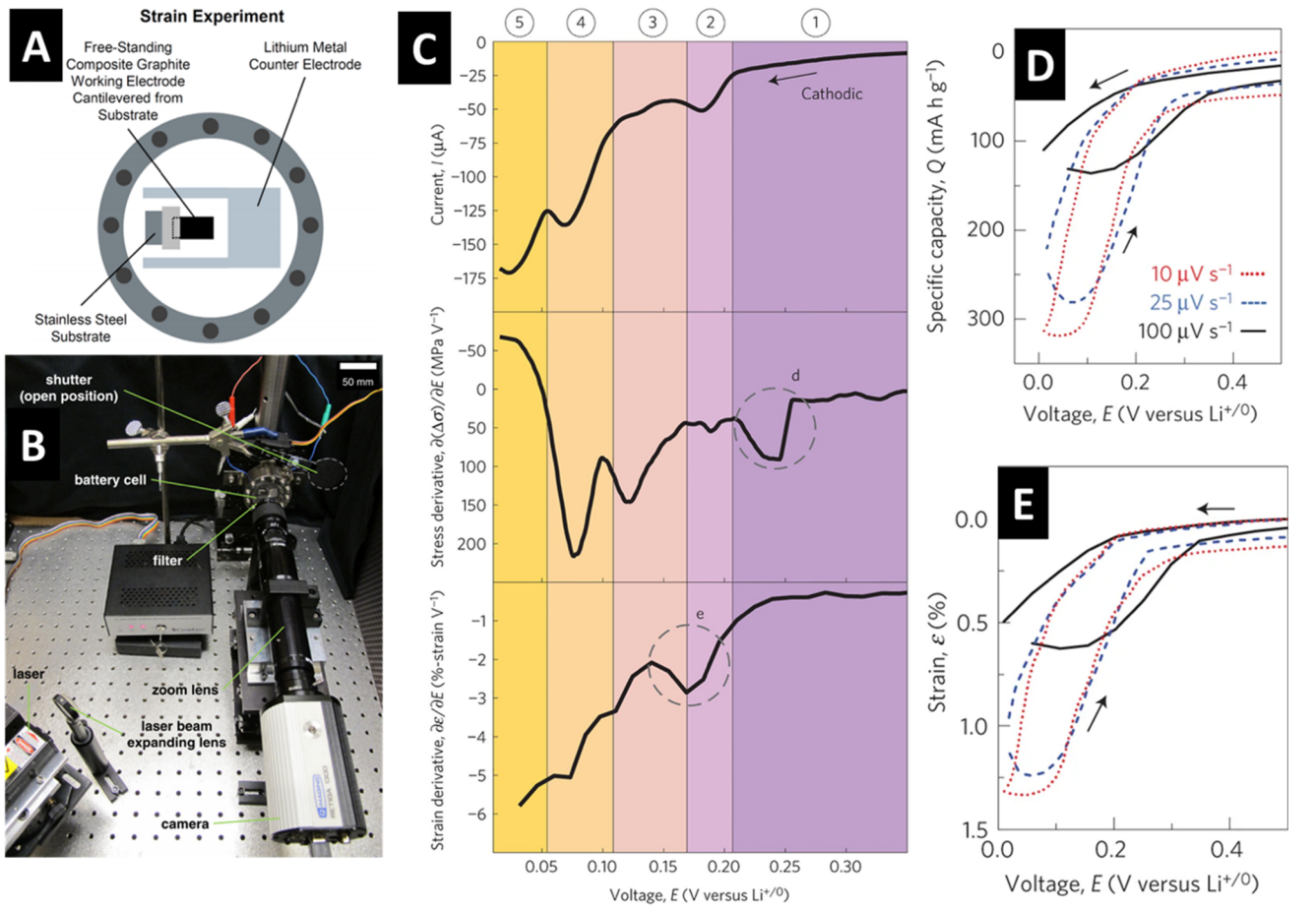

Figure 3. Characterization of Li^+ intercalation and mechanical deformation in a graphite electrode with *operando* electrochemical DIC. (A) Schematic of a custom battery cell used in the strain measurement. Adapted by permission from Springer Nature, ref 46. (B) Imaging setup for DIC measurement. Adapted by permission from Springer Nature, ref 52. (C) (top to bottom) Correlation between cyclic voltammetry current and the potential dependence of the stress and strain derivatives. (D) Specific capacity vs potential at different scan rates. (E) Strain vs potential at the same scan rates as panel D, demonstrating direct correlation between strain and capacity. Adapted by permission from Springer Nature, ref 46.

Arguably the simplest measurement of mechanical deformation in electrochemical cells is via dilatometry techniques. Such methods are ideally suited for probing full electrochemical cells. Dilatometry provides a quick and direct measurement of the overall uniaxial strain in a sealed electrochemical cell and can be adapted for open cell studies. Figure 2A shows a typical

https://dx.doi.org/10.1021/acsenergylett.0c01823
ACS Energy Lett. 2020, 5, 3548−3559

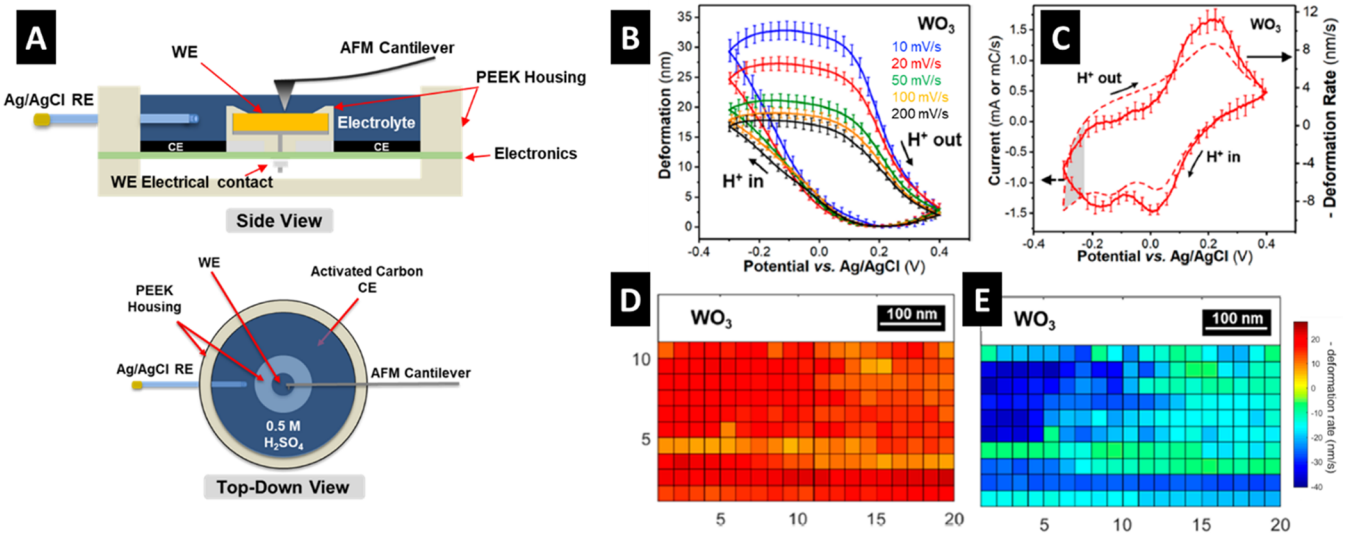

Figure 4. Correlation between proton insertion and mechanical deformation in WO_3 with *operando* electrochemical AFM dilatometry. (A) Schematics of the side and top-down views of an in situ cell for AFM dilatometry. (B) Local electrode deformation as a function of potential at different cyclic voltammetry sweep rates. (C) Cyclic voltammogram and local deformation rate measured via AFM are directly correlated during proton insertion into WO_3. The shaded region indicates current from the onset of the hydrogen evolution reaction. Because this does not contribute to electrode deformation, there is no increase in deformation rate. (D and E) Spatial variation of the deformation rate measured via AFM, at (D) the peak anodic current and (E) the peak cathodic current during proton insertion into WO_3. Adapted with permission from ref 47. Copyright 2018 American Chemical Society.

setup in which a LVDT is used to measure the strain of a Li-ion pouch-cell battery during electrochemical cycling.[48] By simultaneously measuring the strain as a function of time during galvanostatic cycling as well as the voltage, one can correlate the voltage and strain derivatives and elucidate some of the important relationships between strain and electrochemical activity in batteries. For instance, the first derivative of voltage with respect to charge is commonly used to determine aging mechanisms in batteries, yet this approach tends to be limited to slow charging−discharging rates of $C/20$ and below.[66,67] It was found that the second derivative of strain with respect to charge is directly proportional to dV/dQ (Figure 2B) and as such, can be used to shed light on the electrochemical state of the system. The benefit of this approach is that strain is more sensitive at higher currents, thus enabling researchers to understand electrode material evolution under higher charging−discharging rates.

DIC is an optical technique used to measure mechanical properties of single electrodes. A typical cell design and an imaging setup are shown in Figure 3A,B. During the measurement, a fluorescent speckle pattern is projected onto the electrode surface, which serves as the point from which to calculate displacement. It has been used to characterize Li^+ intercalation into graphite (Figure 3C−E) and showed that changes in electrochemical stiffness correlate with the lithiation stage and that the measured stress is proportional to current while strain is proportional to the capacity. The capacity retention at different cyclic voltammetry scan rates (Figure 3D) was directly proportional to the strain (Figure 3E), in agreement with eq 2. In terms of improving rate capability, understanding of this electrochemomechanical coupling led to the proposition that Li^+ intercalation could be faster if the electrode material were designed with lower electrochemical stiffness and insertion-induced stress.[46]

Operando electrochemical AFM dilatometry provides a local measurement of electrode deformation (due to the nanoscale dimensions of an AFM tip) which can be directly linked to global electrochemical information such as stored charge. Figure 4A shows the schematic of a commercial *in situ* three-electrode cell, where the AFM cantilever is placed on the surface of the working electrode (WE) to measure deformation. This technique has been used to study volume expansion of EDLC materials such as carbide-derived carbon and as a function of pore size.[68] In these systems, the electrode volume expands when cations or anions are electrosorbed in the electrode pores. Because of this clear separation of cation and anion behavior, their electrosorption behavior can be studied individually. Most notably is the effect of scan rate where information about the dynamic process is captured by the phase lag between applied potential and electrode response. In the case of ionic liquids, it was shown that the bigger anion inserted more slowly and affected the overall strain response more than the smaller cation.[26] Confined EDL formation in layered materials, such as Ti_3C_2 MXene operating in neutral pH aqueous electrolytes,[69] leads to electrode volume changes that deviate from the parabolic shape found in porous electrodes and depends on the nature of intercalated cation. For example, in aqueous electrolytes, the intercalation of Li ions results in a contraction while the intercalation of K-ions does not result in significant volume changes.[54] This is believed to be a result of the negatively charged MXene surface as well as the uncertain role of solvation shells.

The *operando* AFM technique was also utilized to study redox-active systems, such as proton insertion into WO_3 (Figure 4B), and shows reversible electrode deformation, a hysteresis between the insertion and deinsertion processes, and significant scan rate dependence. The deformation rate was found to be proportional to the current measured from cyclic voltammetry (Figure 4C),[47] in line with eq 4. The maximum deformation rate correlated with the peak current during proton de/insertion, similarly to the DIC results for Li^+ intercalation into graphite. Because of the nanoscale

https://dx.doi.org/10.1021/acsenergylett.0c01823
ACS Energy Lett. 2020, 5, 3548−3559

dimensions of the AFM tip, the technique also allows for mapping of the deformation rate across the electrode surface which could be useful to correlate electrode topography with mechanical deformation (Figure 4D,E).

> Plenty of room remains for exploring novel fast ion electrosorption and insertion materials from a design perspective.

Measurement of electrode stress can also correlate to the kinetics and magnitude of ion electrosorption or insertion charge storage. For example, the MOSS technique measures the curvature of a thin film−substrate system via the reflection of a 1D or 2D array of parallel laser beams from a substrate that is directly imaged with a CCD camera (Figure 5A). If the electrode material is linear elastic, then the measured signal directly maps to the average strain in the film. Likewise, in the case of nonlinear behavior, the measured signal can be mapped to the deformation in the film using an appropriate constitutive model. For electrochemical measurements, this equipment is integrated with custom-built electrochemical cells that contain transparent windows for optical access to characterize thin film electrodes on relatively thick (inactive) substrates. Ion electrosorption and insertion lead to electrode deformation. The thick substrate constrains the in-plane deformation of the relatively thin electrodes, thereby generating in-plane biaxial stresses in the electrodes. These stresses lead to substrate curvature, which causes the laser spots to get farther apart (convex curvature) or closer together (concave curvature). The measured curvature is related to the average in-plane stresses (integrated through the thickness of the film) through Stoney's equation.[70] Overall, the MOSS technique enables monitoring of stresses that develop during electrochemical operation of thin-film battery electrodes.

MOSS has been used to study stresses that arise during electrochemical ion insertion into Li-ion battery electrode materials, including Mn_2O_4[72] and V_2O_5.[71] As one example, Zhang et al. examined the effects of deep discharge of V_2O_5 thin films (Figure 5B). During lithiation, V_2O_5 undergoes several phase transformations as indicated by the distinct potential transitions highlighted with different color backgrounds. The MOSS results indicate that these transformations induce varying levels of stress. The residual stresses remaining after a complete cycle are indicative of plastic deformation, thereby attesting to the irreversibility of the transformation to the γ-$Li_xV_2O_5$ phase. By comparison, shallow discharge (e.g., to 2.8 V vs Li/Li^+) induces primarily elastic deformation, which extends cycle life.

Examples from the four techniques (dilatometry, DIC, AFM, and MOSS) highlight how *operando* deformation measurements can be correlated to electrochemical response of electrochemical cells and electrodes upon ion electrosorption and insertion. A comparison of the techniques is shown in Table 1. Understanding of mechanical deformation can be then used as a guide for the design of entirely new electrosorption and insertion materials with fast kinetics.

Design of Materials for Ion Electrosorption and Insertion with Fast Kinetics. The coupling between ion electrosorption and insertion capacity and deformation could be used to design new materials. One hypothesis is that in order to increase electrosorption or insertion kinetics as well as cycling lifetime, the host material must not undergo significant deformation. As an example, ion electrosorption in EDLCs leads to ~1% electrode deformation and occurs on fast time scales (<30 s) for over a million cycles.[1] The materials design challenge is to identify materials that will store more charge than EDLCs while minimizing deformation. Using this hypothesis as a design strategy, here we describe several structural motifs beyond nanostructuring (crystallographic shear, interlayer pillars, and confined fluids) that have been proposed to minimize deformation during ion electrosorption or insertion with the aim of inspiring new fast charging materials.

Crystallographic Shear. One materials design strategy to minimize electrode deformation is to limit the rotational degrees of freedom of the structural building blocks of the host material. For example, the room-temperature polymorph of WO_3 is a distorted perovskite-like monoclinic structure (γ-WO_3) which consists of corner-sharing WO_6 octahedra.[73] The electrochemical insertion of Li^+ leads to rotations of the WO_6 octahedra as the oxide undergoes several phase transformations en route to the lithiated cubic perovskite $Li_{0.5}WO_3$.[74] A similar phenomenon occurs in ReO_3, which despite metallic conductivity and an open structure, exhibits poor electrochemical cycling stability because of strain associated with the rotation of ReO_6 octahedra during Li^+ de/insertion.[75] Cava et al. hypothesized that such distortions would not occur in crystallographic shear structures of metal oxides which contain

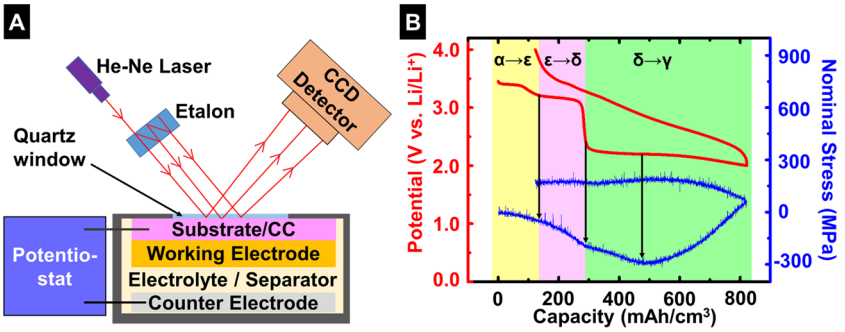

Figure 5. Multibeam optical stress sensor (MOSS) technique for simultaneous electrochemical and stress measurements in thin-film electrodes. (A) Schematic of a typical experimental setup, which employs a laser split through an etalon, a CCD detector, a potentiostat, and an electrochemical cell with a quartz window for optical access. (B) Potential and corresponding stress response during a galvanostatic cycle of a V_2O_5 thin-film electrode between 4.0−2.0 V vs Li/Li^+ at 0.2 C. Adapted with permission of The Royal Society of Chemistry, from ref 71 (permission conveyed through Copyright Clearance Center, Inc.).

https://dx.doi.org/10.1021/acsenergylett.0c01823
ACS Energy Lett. 2020, 5, 3548−3559

Table 1. Comparison of Dilatometry, DIC, AFM, and MOSS Techniques

	dilatometry	DIC	AFM	MOSS
measurement	displacement	displacement	displacement	stress
resolution	μm	μm	nm	MPa
sample requirement	full-cell, nonrigid packaging	free-standing	thin film/slurry electrodes	thin film on reflective substrate
pros	out-of-plane strain measurement	in-plane strain measurement	high resolution, small sample size (single particles)	high resolution, adaptable to any thin film deposition
cons	decoupling active material response from remainder of cell	decoupling active material response from substrate	height sensor drift at long time scales	averages measurement of stress through the thickness of the film; decoupling active material response from substrate

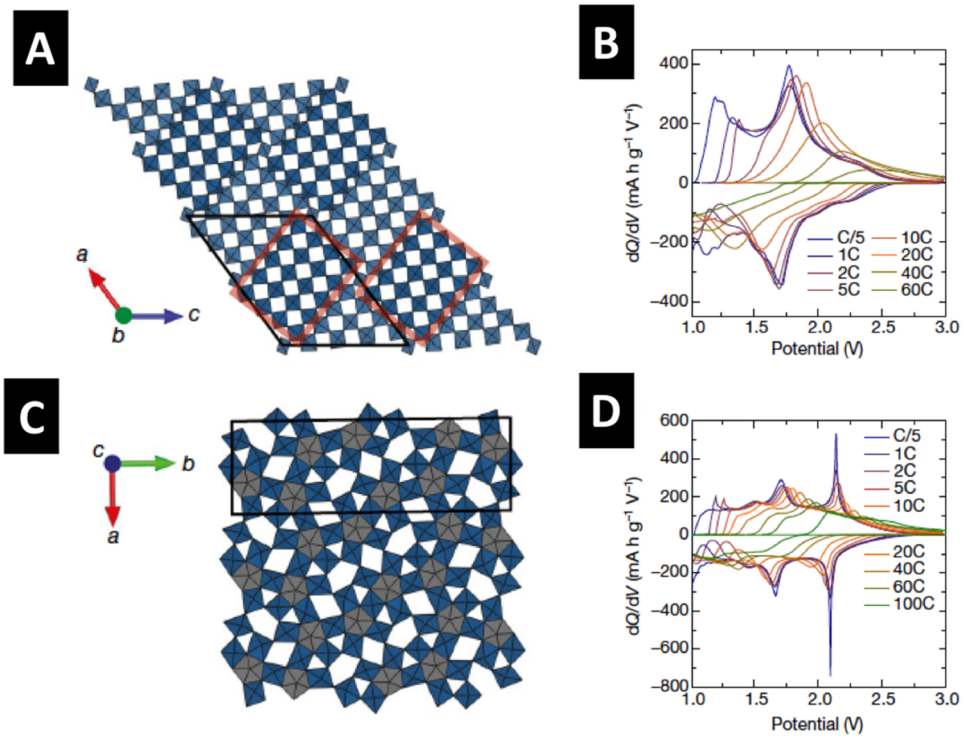

Figure 6. Concept of crystallographic shear to minimize electrode deformation during ion insertion. (a) Crystal structure of $Nb_{16}W_5O_{55}$ with shear planes formed between the building blocks of adjoining 4 × 5 × ∞ $(W,Nb)O_6$ octahedra and $(W,Nb)O_4$ tetrahedra at the corners and (b) its differential capacity vs potential at various *C* rates. (c) Crystal structure of $Nb_{18}W_{16}O_{93}$ formed by 1 × 3 × 1 corner sharing tetragonal tungsten bronze (blue) with pentagonal tunnels partially filled by −W,Nb−O− chains that create pentagonal bipyramids (gray), and d) its differential capacity vs potential at various *C* rates. Adapted from Springer Nature, ref 78. Copyright 2018.

more edge sharing octahedra.[76] Subsequent work by Cava et al. indeed found that crystallographic shear structures of various metal oxides minimized structural distortion but at the expense of the theoretical capacity.[77] More recently, Griffith et al. utilized this strategy to investigate Li^+ insertion into niobium tungsten oxides with crystallographic shear ($Nb_{16}W_5O_{55}$, $Nb_{18}W_{16}O_{93}$; Figure 6).[78] As predicted by Cava et al., they showed that such materials exhibit rapid Li^+ insertion kinetics, ∼3 min charge−discharge in electrodes composed of micrometer scale particles. The importance of a host structure with limited structural rearrangement was again noted as a key factor for achieving such rapid insertion kinetics. A comparison of Li^+ insertion into the perovskite NbO_2F and the shear derivative Nb_3O_7F found that the presence of shear planes led to increased structural stability.[79] The trade-off between structural stability (which determines the kinetics and lifetime) and available insertion sites (which determine capacity) recurs with materials that incorporate structural water, as discussed below.

With more techniques available in today's materials chemists' toolbox, concepts such as crystallographic shear, interlayer pillaring, and confined fluids can be added to and expanded upon.

Interlayer Stabilization via Pillaring. In the case of layered materials, pillaring can help stabilize the structure during ion intercalation. Layered materials are prone to structural conversions that include layer sliding. There are two potential ways in which interlayer pillars can enable stability by minimizing deformation. First, they can essentially "pin" the layers in place so that they do not move past each other. This strategy was used to stabilize $LiMnO_2$, which converts to a spinel structure during electrochemical cycling. It has been proposed that pillaring the layers is possible with large cations

https://dx.doi.org/10.1021/acsenergylett.0c01823
ACS Energy Lett. 2020, 5, 3548−3559

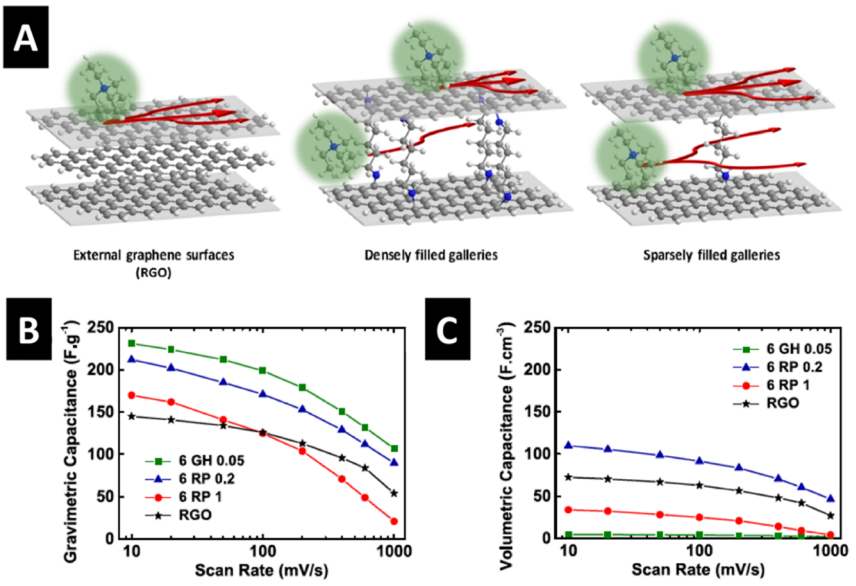

Figure 7. Concept of interlayer stabilization via pillaring to enable ion electrosorption into the galleries of reduced graphene oxide. (A) Schematic of ion transport and structure of reduced pillared graphene materials with no, dense, and sparse interlayer diamine pillars. (B) Gravimetric and (C) volumetric capacitance vs scan rate of reduced graphene oxide (RGO), pillared graphene hydrogel with 0.05 equiv of diamine (6 GH 0.05), and reduced pillared graphene materials with 0.2 and 1 equiv of diamine (6 RP 0.2 and 1). Adapted with permission from ref 87. Copyright 2019 American Chemical Society.

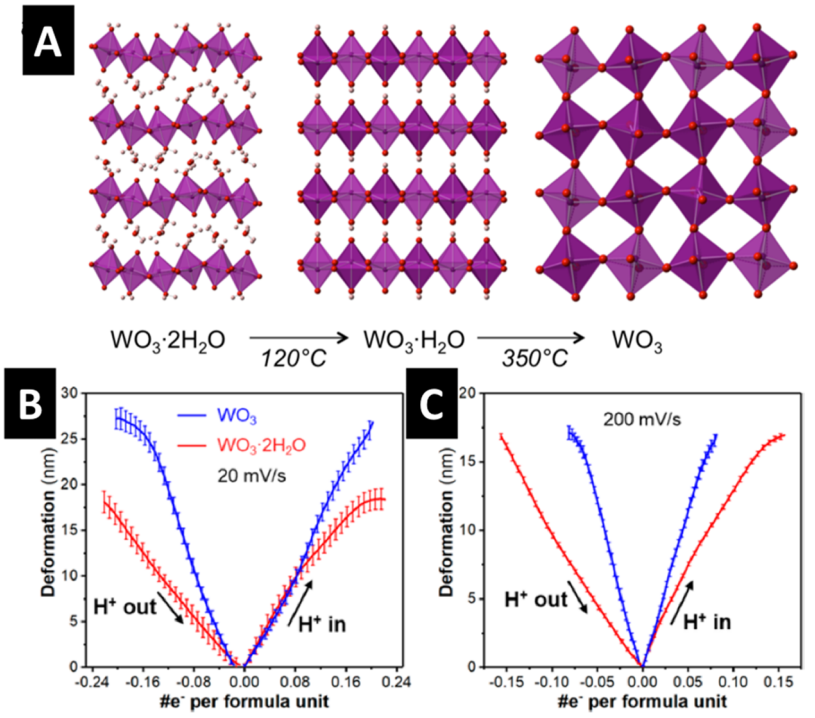

Figure 8. Concept of decreasing electrode deformation by structural water stabilization. (A) Crystal structures of $WO_3 \cdot 2H_2O$, $WO_3 \cdot H_2O$, and WO_3. Deformation vs number of electrons stored per formula unit of $WO_3 \cdot 2H_2O$ and WO_3 at (B) 20 mV s^{-1} and (C) 200 mV s^{-1}, as measured by *operando* AFM dilatometry. Adapted with permission from ref 47. Copyright 2018 American Chemical Society.

such as K^+ to limit Mn^{3+} migration into the interlayer.[3] Both interlayer Zn^{2+} and structural water were used to stabilize the intercalation of Zn^{2+} from an aqueous electrolyte into a layered vanadium oxide bronze.[80] *Operando* XRD analysis indicated that interlayer structural water deintercalated during Zn^{2+} intercalation, while pillaring Zn^{2+} stabilized the layered structure.

Second, the introduction of interlayer pillars can increase the distance between layers to minimize the layer-to-layer interactions and thus decrease deformation. It is proposed that such features enable the intercalation of large or highly polarizable ions (such as multivalent cations) and lead to an overall enhancement in ion transport in the interlayer. An interesting strategy pursued in the field of EDLCs is to utilize pillaring to increase the electrosorption capacity of reduced

https://dx.doi.org/10.1021/acsenergylett.0c01823
ACS Energy Lett. 2020, 5, 3548−3559

graphene oxide.[81−83] Restacking of this material from solution results in an interlayer spacing similar to graphite (ranging between 3.5 and 4 Å)[82] that is inaccessible for the electrosorption of bulky ion electrolytes typically used in double layer capacitors (e.g., tetraethylammonium tetrafluoroborate). Controlled pillaring of reduced graphene oxide with species such as alkyl diamines leads to an increase of the interlayer spacing to 7.8 Å and a concomitant increase of both the gravimetric and volumetric capacitance associated with electrosorption of anions and cations (Figure 7).[83] Similar strategies can be applied to layered materials such as metal chalcogenides, transition metal oxides, and MXenes, highlighting the exciting opportunity to modify the interlayer of existing layered intercalation host materials.[84−86]

Presence of Structural Water and Other Confined Fluids. A related concept to interlayer pillaring is functionalization with confined fluids, which provides exciting opportunities to investigate both fast insertion and electrosorption kinetics and physical properties of fluids under nanoconfinement.[88] The structural water can be present as both secondarily bound water or primarily bound to the lattice ("water of coordination").[89] It is of particular interest to utilize such materials for the insertion of protons because recent *ab initio* molecular dynamics simulations have indicated the presence of Grotthuss-type transport (correlated proton transport along hydrogen bonding networks) even within interlayer confined water.[90] The presence of a hydrogen-bonded structural water network in a Prussian-blue analogue material ($Cu[Fe(CN)_6]_{0.63}\cdot\square_{0.37}\cdot 3.4H_2O$, where $\square$ denotes a $Fe(CN)_6$ vacancy) was proposed to enable rapid (<1 min), diffusion-free electrochemical proton insertion.[91] This material exhibited a solid solution mechanism and only a 2% volume change over the entire extent of proton insertion, in line with the hypothesis that decreased deformation enables fast insertion kinetics. Water confined between sheets of MXenes, 2D materials obtained by selective ion etching of transition metal oxides, has been hypothesized to enable their extremely fast electrochemical proton intercalation kinetics.[92]

Some transition metal oxides contain structural water that is highly confined, as in the case of $WO_3\cdot nH_2O$ (Figure 8) and exhibit very rapid proton insertion kinetics.[93,94] In these materials, the presence of structural water appears to be critical for maintaining structural stability during proton insertion, leading to reduced and more reversible deformation per stored electron, as indicated by *operando* AFM (Figure 8B,C)[47] and XRD results.[94] In particular, structural water seemed to decrease the structural degrees of freedom available for structural deformation during electrochemical insertion, a concept related to the presence of edge-sharing motifs in shear structures described earlier. As with interlayer pillaring, the incorporation of water as well as other types of solvent molecules into the interlayer is a versatile approach for decreasing electrode deformation. It should be noted that the presence of interlayer species can decrease the total available insertion sites and increase the mass of the electrode, so there is still a trade-off between capacity and kinetics.

A structural feature that is closely related to the presence of structural water is structural protonation, where a proton is directly coordinated to a covalently bound oxygen. Fleischmann et al. used a soft chemistry route to prepare a series of hydrogen titanates ($H_2Ti_{3n}O_{6n+1}$, n = 1, 2, 4) and found that significant proton insertion capacity could occur only in the material with the highest degree of structural protonation, $H_2Ti_3O_7$. This was proposed to restrict deformation during proton insertion to one-dimensional interlayer contraction.[95] Structural protons were also hypothesized to open up the crystal structure, which creates more insertion sites and leads to higher capacity.

This Perspective focuses on the fundamental coupling between ion electrosorption and insertion capacity and electrode deformation, its measurement with *operando* techniques, and how it could be used to design new materials with fast kinetics. The development of new *operando* techniques and approaches will play an important role in understanding and evaluating electrode stabilization concepts. Additional effects, such as heat generation (especially at high rates) and the role of external cell pressure can also be studied from the electromechanical perspective. The advancement of measurement brings up the need for developing the corresponding data analysis, where modern statistical tools such as principal component analysis (PCA) and artificial intelligence (AI) can provide valuable insights.[96,97] Plenty of room remains for exploring novel fast ion electrosorption and insertion materials from a design perspective. With more techniques available in today's materials chemists' toolbox, concepts such as crystallographic shear, interlayer pillaring, and confined fluids can be added to and expanded upon. Overall, the understanding of electrosorption and insertion mechanics will shed light on whether it is possible to decouple kinetics, which favor open structures with little distortion, from capacity, which favors dense structures with minimal inactive atoms.

AUTHOR INFORMATION

Corresponding Author

Veronica Augustyn − *Department of Materials Science & Engineering, North Carolina State University, Raleigh, North Carolina 27695, United States;* orcid.org/0000-0001-9885-2882; Email: vaugust@ncsu.edu

Authors

Ruocun Wang − *Department of Materials Science & Engineering, North Carolina State University, Raleigh, North Carolina 27695, United States*

Nina Balke − *Center for Nanophase Materials Sciences, Oak Ridge National Laboratory, Oak Ridge, Tennessee 37830, United States;* orcid.org/0000-0001-5865-5892

Matt Pharr − *Department of Mechanical Engineering, Texas A&M University, College Station, Texas 77843, United States*

Craig B. Arnold − *Department of Mechanical and Aerospace Engineering and Princeton Institute for the Science and Technology of Materials, Princeton University, New Jersey 08540, United States*

Complete contact information is available at: https://pubs.acs.org/10.1021/acsenergylett.0c01823

Notes

The authors declare no competing financial interest.

Biographies

Veronica Augustyn is an Assistant Professor of Materials Science & Engineering and a University Faculty Scholar at North Carolina State University. Her research group focuses on the design, synthesis, and characterization of materials for electrochemical energy technologies. Website: https://www.mse.ncsu.edu/augustyn

https://dx.doi.org/10.1021/acsenergylett.0c01823
ACS Energy Lett. 2020, 5, 3548−3559

Ruocun Wang is a Postdoctoral Fellow in the Department of Materials Science and Engineering at North Carolina State University, working with Prof. Veronica Augustyn. His current research interests include the design, synthesis, and characterization of transition metal oxide hydrates and *operando* characterization of the mechanics of electrochemical intercalation.

Nina Balke is a senior research staff at the Center for Nanophase Materials Sciences at Oak Ridge National Laboratory. She specializes in nanoscale characterization of electromechanical effects and electro-chemo-mechanical coupling using scanning probe microscopy in oxides and vdW layered materials. Website: https://www.ornl.gov/staff-profile/nina-wisinger

Matt Pharr is an Assistant Professor in Mechanical Engineering at Texas A&M University. His research focuses on mechanics of materials, including materials for energy storage and conversion, deformation and fracture of soft materials, mechanics of irradiated materials, coupled electro-chemo-mechanics, and mass transport in materials. Website: https://esml.tamu.edu/

Craig B. Arnold is the Susan Dod Brown Professor of Mechanical and Aerospace Engineering and the Director of the Princeton Institute for the Science and Technology of Materials. His research group focuses on materials processing and characterization for energy storage and conversion with particular emphasis on understanding mechanical phenomena and coupling in these systems. Website: https://spikelab.mycpanel.princeton.edu/

■ ACKNOWLEDGMENTS

V.A., R.W., and N.B. were supported as part of the Fluid Interface Reactions, Structures and Transport (FIRST) Center, an Energy Frontier Research Center funded by the U.S. Department of Energy, Office of Science, Office of Basic Energy Sciences. M.P. acknowledges support from NSF under DMR 1944674. C.B.A. acknowledges support from NSF under CBET-1531871.

■ REFERENCES

(1) Conway, B. E. *Electrochemical Supercapacitors: Scientific Fundamentals and Technological Applications*; Kluwer-Academic: New York, 1999.
(2) Goodenough, J. B.; Park, K.-S. The Li-Ion Rechargeable Battery: A Perspective. *J. Am. Chem. Soc.* **2013**, *135* (4), 1167−1176.
(3) Whittingham, M. Insertion Electrodes as SMART Materials: The First 25 Years and Future Promises. *Solid State Ionics* **2000**, *134* (1−2), 169−178.
(4) Goodenough, J. B.; Manthiram, A. A Perspective on Electrical Energy Storage. *MRS Commun.* **2014**, *4* (4), 135−142.
(5) Lin, Z.; Goikolea, E.; Balducci, A.; Naoi, K.; Taberna, P. L.; Salanne, M.; Yushin, G.; Simon, P. Materials for Supercapacitors: When Li-Ion Battery Power Is Not Enough. *Mater. Today* **2018**, *21* (4), 419−436.
(6) Dunn, B.; Kamath, H.; Tarascon, J.-M. Electrical Energy Storage for the Grid: A Battery of Choices. *Science* **2011**, *334* (6058), 928−935.
(7) Suss, M. E.; Porada, S.; Sun, X.; Biesheuvel, P. M.; Yoon, J.; Presser, V. Water Desalination via Capacitive Deionization: What Is It and What Can We Expect from It? *Energy Environ. Sci.* **2015**, *8*, 2296−2319.
(8) Su, X.; Tan, K.; Elbert, J.; Rüttiger, C.; Gallei, M.; Jamison, T. F.; Hatton, T. A. Asymmetric Faradaic Systems for Selective Electrochemical Separations. *Energy Environ. Sci.* **2017**, *10*, 1272−1283.
(9) Srimuk, P.; Su, X.; Yoon, J.; Aurbach, D.; Presser, V. Charge-Transfer Materials for Electrochemical Water Desalination, Ion Separation and the Recovery of Elements. *Nat. Rev. Mater.* **2020**, *5*, 517−538.
(10) Nadkarni, N.; Zhou, T.; Fraggedakis, D.; Gao, T.; Bazant, M. Z. Modeling the Metal-Insulator Phase Transition in Li_xCoO_2 for Energy and Information Storage. *Adv. Funct. Mater.* **2019**, *29*, 1902821.
(11) Zhu, X.; Li, D.; Liang, X.; Lu, W. D. Ionic Modulation and Ionic Coupling Effects in MoS_2 Devices for Neuromorphic Computing. *Nat. Mater.* **2019**, *18*, 141−148.
(12) Levi, M. D.; Aurbach, D. Frumkin Intercalation Isotherm - a Tool for the Description of Lithium Insertion into Host Materials: A Review. *Electrochim. Acta* **1999**, *45* (1), 167−185.
(13) Gavilán-Arriazu, E. M.; Mercer, M. P.; Pinto, O. A.; Oviedo, O. A.; Barraco, D. E.; Hoster, H. E.; Leiva, E. P. M. Numerical Simulations of Cyclic Voltammetry for Lithium-Ion Intercalation in Nanosized Systems: Finiteness of Diffusion versus Electrode Kinetics. *J. Solid State Electrochem.* **2020**, *24*, 3279.
(14) Whittingham, M. S. Lithium Batteries and Cathode Materials. *Chem. Rev.* **2004**, *104* (10), 4271−4301.
(15) Tivony, R.; Safran, S.; Pincus, P.; Silbert, G.; Klein, J. Charging Dynamics of an Individual Nanopore. *Nat. Commun.* **2018**, *9* (1), 4203.
(16) Hantel, M. M.; Presser, V.; Kötz, R.; Gogotsi, Y. In Situ Electrochemical Dilatometry of Carbide-Derived Carbons. *Electrochem. Commun.* **2011**, *13* (11), 1221−1224.
(17) Kaasik, F.; Tamm, T.; Hantel, M. M.; Perre, E.; Aabloo, A.; Lust, E.; Bazant, M. Z.; Presser, V. Electrochemistry Communications Anisometric Charge Dependent Swelling of Porous Carbon in an Ionic Liquid. *Electrochem. Commun.* **2013**, *34*, 196−199.
(18) Rochester, C. C.; Pruessner, G.; Kornyshev, A. A. Statistical Mechanics of 'Unwanted Electroactuation' in Nanoporous Supercapacitors. *Electrochim. Acta* **2015**, *174*, 978−984.
(19) Sauerteig, D.; Ivanov, S.; Reinshagen, H.; Bund, A. Reversible and Irreversible Dilation of Lithium-Ion Battery Electrodes Investigated by in-Situ Dilatometry. *J. Power Sources* **2017**, *342*, 939−946.
(20) Hantel, M. M.; Weingarth, D.; Kötz, R. Parameters Determining Dimensional Changes of Porous Carbons during Capacitive Charging. *Carbon* **2014**, *69*, 275−286.
(21) Chimola, J.; Yushin, G.; Gogotsi, Y.; Portet, C.; Simon, P.; Taberna, P. L.; Chmiola, J.; Yushin, G.; Gogotsi, Y.; Portet, C.; et al. Anomalous Increase in Carbon Capacitance at Pore Sizes Less than 1 Nanometer. *Science* **2006**, *313* (5794), 1760−1763.
(22) Simon, P.; Gogotsi, Y. Charge Storage Mechanism in Nanoporous Carbons and Its Consequence for Electrical Double Layer Capacitors. *Philos. Trans. R. Soc., A* **2010**, *368*, 3457−3467.
(23) Futamura, R.; Iiyama, T.; Takasaki, Y.; Gogotsi, Y.; Biggs, M. J.; Salanne, M.; Ségalini, J.; Simon, P.; Kaneko, K. Partial Breaking of the Coulombic Ordering of Ionic Liquids Confined in Carbon Nanopores. *Nat. Mater.* **2017**, *16*, 1225−1232.
(24) Biesheuvel, P. M.; Porada, S.; Levi, M.; Bazant, M. Z. Attractive Forces in Microporous Carbon Electrodes for Capacitive Deionization. *J. Solid State Electrochem.* **2014**, *18* (5), 1365−1376.
(25) Koczwara, C.; Rumswinkel, S.; Prehal, C.; Jäckel, N.; Elsässer, M. S.; Amenitsch, H.; Presser, V.; Hüsing, N.; Paris, O. In Situ Measurement of Electrosorption-Induced Deformation Reveals the Importance of Micropores in Hierarchical Carbons. *ACS Appl. Mater. Interfaces* **2017**, *9* (28), 23319−23324.
(26) Black, J. M.; Feng, G.; Fulvio, P. F.; Hillesheim, P. C.; Dai, S.; Gogotsi, Y.; Cummings, P. T.; Kalinin, S. V.; Balke, N. Strain-Based in Situ Study of Anion and Cation Insertion into Porous Carbon Electrodes with Different Pore Sizes. *Adv. Energy Mater.* **2014**, *4* (3), 1300683.
(27) Hahn, M.; Barbieri, O.; Campana, F. P.; Kötz, R.; Gallay, R. Carbon Based Double Layer Capacitors with Aprotic Electrolyte Solutions: The Possible Role of Intercalation/Insertion Processes. *Appl. Phys. A: Mater. Sci. Process.* **2006**, *82* (4), 633−638.
(28) Yang, Y. D.; Moon, G. J.; Oh, J. M.; Kang, I. S. Discrete and Continuum Analyses of Confinement Effects of an Ionic Liquid on the EDL Structure and the Pressure Acting on the Wall. *J. Phys. Chem. C* **2019**, *123* (4), 2516−2525.
(29) Hooley, J. G. Physical Chemistry and Mechanism of Intercalation in Graphite. *Mater. Sci. Eng.* **1977**, *31* (C), 17−24.

https://dx.doi.org/10.1021/acsenergylett.0c01823
ACS Energy Lett. 2020, 5, 3548−3559

(30) Whittingham, M. S.; Jacobson, A. J. *Intercalation Chemistry*; Academic Press: New York, 1982.
(31) Astruc, D. Why Is Ferrocene so Exceptional? *Eur. J. Inorg. Chem.* **2017**, *2017* (1), 6−29.
(32) Eiland, P. F.; Pepinsky, R. X-Ray Examination of Iron Biscyclopentadienyl. *J. Am. Chem. Soc.* **1952**, *74* (19), 4971.
(33) Kotak, N.; Barai, P.; Verma, A.; Mistry, A.; Mukherjee, P. P. Electrochemistry-Mechanics Coupling in Intercalation Electrodes. *J. Electrochem. Soc.* **2018**, *165* (5), A1064−A1083.
(34) Zhao, K.; Pharr, M.; Vlassak, J. J.; Suo, Z. Fracture of Electrodes in Lithium-Ion Batteries Caused by Fast Charging. *J. Appl. Phys.* **2010**, *108* (7), 073517.
(35) Xu, R.; Zhao, K. Electrochemomechanics of Electrodes in Li-Ion Batteries: A Review. *J. Electrochem. Energy Convers. Storage* **2016**, *13* (3), 030803.
(36) Wu, B.; Lu, W. A Battery Model That Fully Couples Mechanics and Electrochemistry at Both Particle and Electrode Levels by Incorporation of Particle Interaction. *J. Power Sources* **2017**, *360*, 360−372.
(37) Christensen, J.; Newman, J. Stress Generation and Fracture in Lithium Insertion Materials. *J. Solid State Electrochem.* **2006**, *10*, 293−319.
(38) Zhang, X.; Shyy, W.; Marie Sastry, A. Numerical Simulation of Intercalation-Induced Stress in Li-Ion Battery Electrode Particles. *J. Electrochem. Soc.* **2007**, *154* (10), A910.
(39) Cheng, Y. T.; Verbrugge, M. W. Evolution of Stress within a Spherical Insertion Electrode Particle under Potentiostatic and Galvanostatic Operation. *J. Power Sources* **2009**, *190* (2), 453−460.
(40) Golmon, S.; Maute, K.; Lee, S. H.; Dunn, M. L. Stress Generation in Silicon Particles during Lithium Insertion. *Appl. Phys. Lett.* **2010**, *97* (3), 033111.
(41) Sethuraman, V. A.; Srinivasan, V.; Bower, A. F.; Guduru, P. R. In Situ Measurements of Stress-Potential Coupling in Lithiated Silicon. *J. Electrochem. Soc.* **2010**, *157* (11), A1253−A1261.
(42) Cannarella, J.; Leng, C. Z.; Arnold, C. B. On the Coupling Between Stress and Voltage in Lithium Ion Pouch Cells. *Proc. SPIE* **2014**, *9115*, 91150K.
(43) Cannarella, J.; Arnold, C. B. The Effects of Defects on Localized Plating in Lithium-Ion Batteries. *J. Electrochem. Soc.* **2015**, *162* (7), A1365−A1373.
(44) Liu, X. M.; Fang, A.; Haataja, M. P.; Arnold, C. B. Size Dependence of Transport Non-Uniformities on Localized Plating in Lithium-Ion Batteries. *J. Electrochem. Soc.* **2018**, *165* (5), A1147−A1155.
(45) Woodford, W. H.; Carter, W. C.; Chiang, Y. M. Design Criteria for Electrochemical Shock Resistant Battery Electrodes. *Energy Environ. Sci.* **2012**, *5* (7), 8014−8024.
(46) Tavassol, H.; Jones, E. M. C.; Sottos, N. R.; Gewirth, A. A. Electrochemical Stiffness in Lithium-Ion Batteries. *Nat. Mater.* **2016**, *15* (11), 1182−1188.
(47) Wang, R.; Mitchell, J. B.; Gao, Q.; Tsai, W.; Boyd, S.; Pharr, M.; Balke, N.; Augustyn, V. Operando Atomic Force Microscopy Reveals Mechanics of Structural Water Driven Battery-to-Pseudocapacitor Transition. *ACS Nano* **2018**, *12*, 6032−6039.
(48) Schiffer, Z. J.; Cannarella, J.; Arnold, C. B. Strain Derivatives for Practical Charge Rate Characterization of Lithium Ion Electrodes. *J. Electrochem. Soc.* **2016**, *163* (3), A427.
(49) Mukhopadhyay, A.; Sheldon, B. W. Deformation and Stress in Electrode Materials for Li-Ion Batteries. *Prog. Mater. Sci.* **2014**, *63*, 58−116.
(50) Jangid, M. K.; Mukhopadhyay, A. Real-Time Monitoring of Stress Development during Electrochemical Cycling of Electrode Materials for Li-Ion Batteries: Overview and Perspectives. *J. Mater. Chem. A* **2019**, *7* (41), 23679−23726.
(51) Cheng, X.; Pecht, M. In Situ Stress Measurement Techniques on Li-Ion Battery Electrodes: A Review. *Energies* **2017**, *10* (5), 591.
(52) Jones, E. M. C.; Silberstein, M. N.; White, S. R.; Sottos, N. R. In Situ Measurements of Strains in Composite Battery Electrodes during Electrochemical Cycling. *Exp. Mech.* **2014**, *54* (6), 971−985.
(53) Çapraz, Ö. Ö.; Bassett, K. L.; Gewirth, A. A.; Sottos, N. R. Electrochemical Stiffness Changes in Lithium Manganese Oxide Electrodes. *Adv. Energy Mater.* **2017**, *7*, 1601778.
(54) Come, J.; Black, J. M.; Lukatskaya, M. R.; Naguib, M.; Beidaghi, M.; Rondinone, A. J.; Kalinin, S. V.; Wesolowski, D. J.; Gogotsi, Y.; Balke, N. Controlling the Actuation Properties of MXene Paper Electrodes upon Cation Intercalation. *Nano Energy* **2015**, *17*, 27−35.
(55) Come, J.; Xie, Y.; Naguib, M.; Jesse, S.; Kalinin, S. V.; Gogotsi, Y.; Kent, P. R. C.; Balke, N. Nanoscale Elastic Changes in 2D Ti3C2Tx (MXene) Pseudocapacitive Electrodes. *Adv. Energy Mater.* **2016**, *6*, 1502290.
(56) Huang, J. Y.; Zhong, L.; Wang, C. M.; Sullivan, J. P.; Xu, W.; Zhang, L. Q.; Mao, S. X.; Hudak, N. S.; Liu, X. H.; Subramanian, A.; et al. In Situ Observation of the Electrochemical Lithiation of a Single SnO_2 Nanowire Electrode. *Science* **2010**, *330* (6010), 1515−1520.
(57) Wang, C.-M. In Situ Transmission Electron Microscopy and Spectroscopy Studies of Rechargeable Batteries under Dynamic Operating Conditions: A Retrospective and Perspective View. *J. Mater. Res.* **2015**, *30* (03), 326−339.
(58) Baudry, P.; Armand, M.; Gauthier, M.; Masounave, J. In Situ Observation by SEM of Positive Composite Electrodes during Discharge of Polymer Lithium Batteries. *Solid State Ionics* **1988**, *28−30* (PART 2), 1567−1571.
(59) Tippens, J.; Miers, J. C.; Afshar, A.; Lewis, J. A.; Cortes, F. J. Q.; Qiao, H.; Marchese, T. S.; Di Leo, C. V.; Saldana, C.; McDowell, M. T. Visualizing Chemomechanical Degradation of a Solid-State Battery Electrolyte. *ACS Energy Lett.* **2019**, *4* (6), 1475−1483.
(60) Eastwood, D. S.; Yufit, V.; Gelb, J.; Gu, A.; Bradley, R. S.; Harris, S. J.; Brett, D. J. L.; Brandon, N. P.; Lee, P. D.; Withers, P. J.; et al. Lithiation-Induced Dilation Mapping in a Lithium-Ion Battery Electrode by 3D X-Ray Microscopy and Digital Volume Correlation. *Adv. Energy Mater.* **2014**, *4* (4), 1300506.
(61) Ebner, M.; Marone, F.; Stampanoni, M.; Wood, V. Visualization and Quantification of Electrochemical and Mechanical Degradation in Li Ion Batteries. *Science* **2013**, *342*, 716.
(62) Lin, F.; Liu, Y.; Yu, X.; Cheng, L.; Singer, A.; Shpyrko, O. G. G.; Xin, H. L. L.; Tamura, N.; Tian, C.; Weng, T. C. T.-C. Synchrotron X-Ray Analytical Techniques for Studying Materials Electrochemistry in Rechargeable Batteries. *Chem. Rev.* **2017**, *117* (21), 13123.
(63) Kru, B.; Aken Van, K. L.; Alhabeb, M.; Anasori, B.; Jäckel, N.; Krüner, B.; Van Aken, K. L.; Alhabeb, M.; Anasori, B.; Kaasik, F.; et al. Electrochemical in Situ Tracking of Volumetric Changes in Two-Dimensional Metal Carbides (MXenes) in Ionic Liquids. *ACS Appl. Mater. Interfaces* **2016**, *8* (47), 32089−32093.
(64) Levi, M. D.; Daikhin, L.; Aurbach, D.; Presser, V. Quartz Crystal Microbalance with Dissipation Monitoring (EQCM-D) for in-Situ Studies of Electrodes for Supercapacitors and Batteries: A Mini-Review. *Electrochem. Commun.* **2016**, *67*, 16−21.
(65) Levi, M. D.; Lukatskaya, M. R.; Sigalov, S.; Beidaghi, M.; Shpigel, N.; Daikhin, L.; Aurbach, D.; Barsoum, M. W.; Gogotsi, Y. Solving the Capacitive Paradox of 2D MXene Using Electrochemical Quartz-Crystal Admittance and in Situ Electronic Conductance Measurements. *Adv. Energy Mater.* **2015**, *5* (1), 1400815.
(66) Dahn, H. M.; Smith, A. J.; Burns, J. C.; Stevens, D. A.; Dahn, J. R. User-Friendly Differential Voltage Analysis Freeware for the Analysis of Degradation Mechanisms in Li-Ion Batteries. *J. Electrochem. Soc.* **2012**, *159* (9), A1405−A1409.
(67) Deshpande, R.; Verbrugge, M.; Cheng, Y.-T.; Wang, J.; Liu, P. Battery Cycle Life Prediction with Coupled Chemical Degradation and Fatigue Mechanics. *J. Electrochem. Soc.* **2012**, *159* (10), A1730−A1738.
(68) Arruda, T. M.; Heon, M.; Presser, V.; Hillesheim, P. C.; Dai, S.; Gogotsi, Y.; Kalinin, S. V.; Balke, N. In Situ Tracking of the Nanoscale Expansion of Porous Carbon Electrodes. *Energy Environ. Sci.* **2013**, *6*, 225−231.
(69) Gao, Q.; Sun, W.; Ilani-Kashkouli, P.; Tselev, A.; Kent, P.; Kabengi, N.; Naguib, M.; Alhabeb, M.; Tsai, W.-Y.; Baddorf, A.; et al.

https://dx.doi.org/10.1021/acsenergylett.0c01823
ACS Energy Lett. 2020, 5, 3548−3559

Tracking Ion Intercalation into Layered Ti_3C_2 MXene Films across Length Scales. *Energy Environ. Sci.* **2020**, *13*, 2549−2558.
(70) Stoney, G. G. The Tension o f Metallic Films Deposited by Electrolysis. *Proc. R. Soc. A* **1909**, *82* (553), 172−175.
(71) Zhang, Y.; Luo, Y.; Fincher, C.; Banerjee, S.; Pharr, M. Chemo-Mechanical Degradation in V_2O_5 Thin Film Cathodes of Li-Ion Batteries during Electrochemical Cycling. *J. Mater. Chem. A* **2019**, *7* (41), 23922−23930.
(72) Sheth, J.; Karan, N. K.; Abraham, D. P.; Nguyen, C. C.; Lucht, B. L.; Sheldon, B. W.; Guduru, P. R. In Situ Stress Evolution in $Li_{1+x}Mn_2O_4$ Thin Films during Electrochemical Cycling in Li-Ion Cells. *J. Electrochem. Soc.* **2016**, *163* (13), A2524−A2530.
(73) Zheng, H.; Ou, J. Z.; Strano, M. S.; Kaner, R. B.; Mitchell, A.; Kalantar-Zadeh, K. Nanostructured Tungsten Oxide - Properties, Synthesis, and Applications. *Adv. Funct. Mater.* **2011**, *21* (12), 2175−2196.
(74) Granqvist, C. G. Bulk Crystalline Tungsten Oxide. In *Handbook of Inorganic Electrochromic Materials*; Elsevier; Amsterdam, 2002; pp 19−27.
(75) Bashian, N. H.; Zhou, S.; Zuba, M.; Ganose, A. M.; Stiles, J. W.; Ee, A.; Ashby, D. S.; Scanlon, D. O.; Piper, L. F. J.; Dunn, B.; et al. Correlated Polyhedral Rotations in the Absence of Polarons during Electrochemical Insertion of Lithium in ReO_3. *ACS Energy Lett.* **2018**, *3* (10), 2513−2519.
(76) Cava, R. J.; Santoro, A.; Murphy, D. W.; Zahurak, S. M.; Roth, R. S. The Structures of the Lithium Inserted Metal Oxides $Li_{0.2}ReO_3$ and $Li_{0.36}WO_3$. *J. Solid State Chem.* **1983**, *50* (1), 121−128.
(77) Cava, R. J.; Murphy, D. W.; Zahurak, S. Lithium Insertion in Wadsley-Roth Phases Based on Niobium Oxide. *J. Electrochem. Soc.* **1983**, *130* (12), 2345−2351.
(78) Griffith, K. J.; Wiaderek, K. M.; Cibin, G.; Marbella, L. E.; Grey, C. P. Niobium Tungsten Oxides for High-Rate Lithium-Ion Energy Storage. *Nature* **2018**, *559* (7715), 556−563.
(79) Bashian, N. H.; Preefer, M. B.; Milam-Guerrero, J.; Zak, J. J.; Sendi, C.; Ahsan, S. A.; Vincent, R. C.; Haiges, R.; See, K. A.; Seshadri, R.; Melot, B. C. Understanding the Role of Crystallographic Shear on the Electrochemical Behavior of Niobium Oxyfluorides. *J. Mater. Chem. A* **2020**, *8*, 12623−12632.
(80) Kundu, D.; Adams, B. D.; Duffort, V.; Vajargah, S. H.; Nazar, L. F. A High-Capacity and Long-Life Aqueous Rechargeable Zinc Battery Using a Metal Oxide Intercalation Cathode. *Nat. Energy* **2016**, *1*, 16119.
(81) Banda, H.; Périé, S.; Daffos, B.; Dubois, L.; Crosnier, O.; Simon, P.; Taberna, P. L.; Duclairoir, F. Investigation of Ion Transport in Chemically Tuned Pillared Graphene Materials through Electrochemical Impedance Analysis. *Electrochim. Acta* **2019**, *296*, 882−890.
(82) Banda, H.; Daffos, B.; Périé, S.; Chenavier, Y.; Dubois, L.; Aradilla, D.; Pouget, S.; Simon, P.; Crosnier, O.; Taberna, P.-L.; et al. Ion Sieving Effects in Chemically Tuned Pillared Graphene Materials for Electrochemical Capacitors. *Chem. Mater.* **2018**, *30*, 3040−3047.
(83) Banda, H.; Perie, S.; Daffos, B.; Taberna, P.-L.; Dubois, L.; Crosnier, O.; Simon, P.; Lee, D.; De Paepe, G.; Duclairoir, F. Sparsely Pillared Graphene Materials for High- Performance Supercapacitors: Improving Ion Transport and Storage Capacity. *ACS Nano* **2019**, *13*, 1443−1453.
(84) Augustyn, V. Tuning the Interlayer of Transition Metal Oxides for Electrochemical Energy Storage. *J. Mater. Res.* **2017**, *32* (1), 2−15.
(85) Xue, Y.; Zhang, Q.; Wang, W.; Cao, H.; Yang, Q.; Fu, L. Opening Two-Dimensional Materials for Energy Conversion and Storage: A Concept. *Adv. Energy Mater.* **2017**, *7*, 1602684.
(86) Wan, J.; Lacey, S. D.; Dai, J.; Bao, W.; Fuhrer, M. S.; Hu, L. Tuning Two-Dimensional Nanomaterials by Intercalation: Materials, Properties and Applications. *Chem. Soc. Rev.* **2016**, *45*, 6742−6765.
(87) Banda, H.; Périé, S.; Daffos, B.; Taberna, P. L.; Dubois, L.; Crosnier, O.; Simon, P.; Lee, D.; De Paëpe, G.; Duclairoir, F. Sparsely Pillared Graphene Materials for High-Performance Supercapacitors: Improving Ion Transport and Storage Capacity. *ACS Nano* **2019**, *13* (2), 1443−1453.
(88) Augustyn, V.; Gogotsi, Y. 2D Materials with Nanoconfined Fluids for Electrochemical Energy Storage. *Joule* **2017**, *1* (3), 443−452.
(89) Bunker, B. C.; Casey, W. H. *The Aqueous Chemistry of Oxides*; Oxford University Press: New York, 2016.
(90) Muñoz-Santiburcio, D.; Wittekindt, C.; Marx, D. Nanoconfinement Effects on Hydrated Excess Protons in Layered Materials. *Nat. Commun.* **2013**, *4*, 2349.
(91) Wu, X.; Hong, J. J.; Shin, W.; Ma, L.; Liu, T.; Bi, X.; Yuan, Y.; Qi, Y.; Surta, T. W.; Huang, W.; et al. Diffusion-Free Grotthuss Topochemistry for High-Rate and Long-Life Proton Batteries. *Nat. Energy 2019* **2019**, *4*, 123−130.
(92) Lukatskaya, M. R.; Kota, S.; Lin, Zi.; Zhao, M.-Q.; Shpigel, N.; Levi, M. D.; Halim, J.; Taberna, P.-L.; Barsoum, M. W.; Simon, P.; et al. Ultra-High-Rate Pseudocapacitive Energy Storage in Two-Dimensional Transition Metal Carbides. *Nat. Energy* **2017**, *2*, 17105.
(93) Mitchell, J. B.; Lo, W. C.; Genc, A.; LeBeau, J.; Augustyn, V. Transition from Battery to Pseudocapacitor Behavior via Structural Water in Tungsten Oxide. *Chem. Mater.* **2017**, *29*, 3928−3937.
(94) Mitchell, J. B.; Geise, N. R.; Paterson, A. R.; Osti, N. C.; Sun, Y.; Fleischmann, S.; Zhang, R.; Madsen, L. A.; Toney, M. F.; Jiang, D.; et al. Confined Interlayer Water Promotes Structural Stability for High-Rate Electrochemical Proton Intercalation in Tungsten Oxide Hydrates. *ACS Energy Lett.* **2019**, *4*, 2805−2812.
(95) Fleischmann, S.; Sun, Y.; Osti, N. C.; Wang, R.; Mamontov, E.; Jiang, D. E.; Augustyn, V. Interlayer Separation in Hydrogen Titanates Enables Electrochemical Proton Intercalation. *J. Mater. Chem. A* **2020**, *8* (1), 412−421.
(96) Bonnet, N. Some Trends in Microscope Image Processing. *Micron* **2004**, *35* (8), 635−653.
(97) Kalinin, S. V.; Lupini, A. R.; Dyck, O.; Jesse, S.; Ziatdinov, M.; Vasudevan, R. K. Lab on a Beam-Big Data and Artificial Intelligence in Scanning Transmission Electron Microscopy. *MRS Bull.* **2019**, *44* (7), 565−575.

https://dx.doi.org/10.1021/acsenergylett.0c01823
ACS Energy Lett. 2020, 5, 3548−3559